



Cite this: *Phys. Chem. Chem. Phys.*,
2016, **18**, 18678

Received 30th May 2016,
Accepted 23rd June 2016

DOI: 10.1039/c6cp04377a

www.rsc.org/pccp

Molecular design of light-harvesting photosensitizers: effect of varied linker conjugation on interfacial electron transfer†

Jianbing Jiang,‡ John R. Swierk,‡ Svante Hedström, Adam J. Matula, Robert H. Crabtree,* Victor S. Batista,* Charles A. Schmuttenmaer* and Gary W. Brudvig*

Interfacial electron transfer dynamics of a series of photosensitizers bound to TiO₂ via linkers of varying conjugation strength are explored by spectroscopic and computational techniques. Injection and recombination depend on the extent of conjugation in the linker, where the LUMO delocalization determines the injection dynamics but both the HOMO and HOMO–1 are involved in recombination.

The efficient capture and conversion of solar energy into a usable form is a significant research target. Dye-sensitized systems, such as dye-sensitized solar cells (DSSCs) and water-splitting dye-sensitized photoelectrochemical cells (WS-DSPECs), utilize high surface area metal oxide scaffolds sensitized with a molecular light-absorbing dye to harvest sunlight and convert it into an electrical potential *via* an electron-transfer event between the sensitizer and a metal oxide. A solution-phase redox shuttle quenches the sensitizer radical in DSSCs, while in WS-DSPECs it is quenched by a water oxidation catalyst.^{1,2} Unfortunately, in WS-DSPECs and p-type DSSCs, rapid back electron transfer (recombination) significantly limits the power conversion efficiencies that can be attained.^{3,4}

Molecular design offers a promising strategy for tuning the interfacial electron-transfer kinetics in dye-sensitized energy-conversion systems. In DSSCs, a substantial research effort has explored systems of donor–acceptor dyes where the donor–acceptor pair is bridged by a π -conjugated system and has led to significant improvements in power-conversion efficiencies.^{5–7} Alternatively, positioning saturated alkyl linkers between chromophores and anchoring groups is effective at retarding detrimental recombination.⁸ The intermediate case, where the chromophore

and anchor are connected by a partially conjugated bridge, is largely unexplored.

Recently, we demonstrated a phenyl-amide structure that functions as a molecular rectifier based on the spatial asymmetry of the amide moiety.⁹ The amide partially breaks the conjugation within the molecule and depending on its orientation, moves the LUMO closer or further from the Fermi level of the system, making it sensitive to the bias potential and thereby imparting rectifying character.

Inspired by these rectifiers, we developed a novel series of dyes (**Ru1–Ru3**, Chart 1), as a platform for exploring partially conjugated linking strategies using spectroscopic techniques to characterize the interfacial electron-transfer dynamics in conjunction with quantum chemistry calculations. The dyes, based on the well studied ruthenium tris(bipyridine) motif, were prepared by a standard synthetic strategy, starting with the preparation of the functionalized bipyridine intermediates bearing an ethyl phosphonate group and incorporating amide or ethylene units. The amide bonds were then formed by coupling an amine unit to the carboxylic acid, pre-activated with thionyl chloride for **Amide1** or carbodiimide for **Amide2**. The alkene was formed by condensation of a phosphonate and aldehyde in a Horner–Wadsworth–Emmons reaction. In the next step, the ruthenium tris(bipyridine) complex was synthesized and subjected to chloride-to-PF₆[–] anion exchange for better solubility. Finally, removal of the ethyl groups unveiled the phosphonate anchoring groups. Each target compound was prepared in

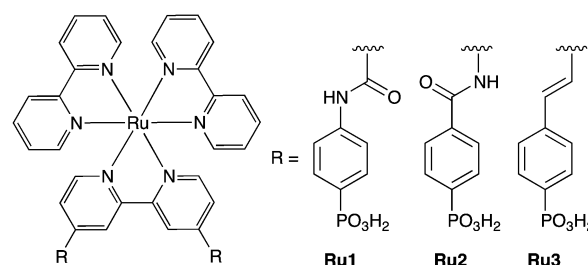


Chart 1 Light-harvesting sensitizers explored in this study.

Department of Chemistry and Energy Sciences Institute, Yale University, New Haven, Connecticut, 06520, USA. E-mail: robert.crabtree@yale.edu, victor.batista@yale.edu, charles.schmuttenmaer@yale.edu, gary.brudvig@yale.edu
† Electronic supplementary information (ESI) available: Full experimental and computational details, including synthetic route, DFT calculations, electron dynamics calculations, Marcus recombination calculations, etc. See DOI: 10.1039/c6cp04377a
‡ Equal contributions.



modest to high yields, and fully characterized prior to use. Phosphonate groups were used to anchor the chromophores to TiO₂ because of their high stability in aqueous environments.¹⁰

Fig. S1 (ESI[†]) shows the steady-state absorption spectra of **Ru1-ester**, **Ru2-ester**, and **Ru3-ester** in acetonitrile. As is typical of ruthenium tris(bipyridine) derivatives, the only absorption feature in the visible region is a strong metal-to-ligand charge-transfer band. For **Ru3-ester**, the absorption is notably stronger and slightly broader, attributed to the stronger delocalization across the linker. The steady-state emission spectra for the three ester compounds show broad emissions at wavelengths longer than 550 nm. For this class of compounds, the heavy Ru atom induces spin-orbit coupling, facilitating rapid and nearly quantitative intersystem crossing of the excited singlet (S₁) to the triplet (T₁), with subsequent emission from the T₁ state. By fitting the emission spectra to a single-mode Franck-Condon function,^{11,12} the energy gap (E₀₋₀) between the zeroth vibrational levels of the S₀ and T₁ states can be determined, see Fig. 1 and Table S1 (ESI[†]). The E₀₋₀ values are similar (~2 eV) for the three compounds. Table S1 (ESI[†]) also shows the vertical transition energies for S₀ → S₁ calculated with linear-response time-dependent DFT as well as the energy difference between the T₁ and S₀ states after optimization with unrestricted DFT (uDFT). Details of the calculations are found in the ESI.[†] In general, the agreement between the experimental and calculated E₀₋₀(S₀ → T₁) values is very good, differing by less than 0.1 eV in all cases. While S₁ → S₀ emission cannot be observed experimentally, hot injection from the S₁ state into TiO₂ is known to occur for other ruthenium tris(bipyridine) derivatives.¹³ DFT calculations suggest that the unrelaxed S₁ state of these compounds lies above the optimized T₁ by about 0.5 eV.

The ground state potential for oxidation E_{1/2}(Ru^{3+/2+}) was determined from cyclic voltammetry in acetonitrile using the ester versions of **Ru1**, **Ru2**, and **Ru3** (Fig. S2, ESI[†]) and was also calculated with uDFT. For **Ru1-ester**, we determined a potential of 1.32 V vs. NHE, while **Ru2-ester** and **Ru3-ester** gave potentials of 1.06 V and 1.21 V vs. NHE, respectively (Table S1, ESI[†]). The excited state reduction potential E^{0/}(Ru^{3+/2+*}) can be approximated

as the difference between E_{1/2}(Ru^{3+/2+}) and E₀₋₀ (Fig. 1). **Ru2** exhibits the most negative E_{1/2}(Ru^{3+/2+*}) at -1.06 V vs. NHE, while **Ru1** and **Ru3** lie lower in energy at -0.63 and -0.72 V vs. NHE, respectively. At pH 1, there is significant ΔG for injection into the conduction band of at least 420 mV. The calculated T₁ excited-state energies are slightly but consistently underestimated compared to experiments, which correlates with the small underestimations of the reduction potentials. (Fig. S1 and Table S1, ESI[†]).

The relative energy levels of the three compounds are rationalized from their chemical structures as follows. The carbonyl group directly attached to the bpy in **Ru1** is electron-withdrawing and consequently stabilizes the orbitals in the bpy π system. In **Ru2**, however, the electron-donating amine group raises the bpy π-orbital energies. This has a larger effect on the LUMOs, which are of pure π* character, than on the HOMOs that are mainly Ru-d orbitals but have some bpy-π character. The HOMO level directly relates to the ground state potential for oxidation, and the LUMO level relates to the excited state potential since the excitation predominantly corresponds to the promotion of an electron to this orbital. **Ru3** exhibits intermediate potentials in all cases due to the very weakly electron-donating vinylene group. The calculated HOMO, LUMO, and HOMO-1 of all dyes are depicted in Fig. 2.

Time-resolved terahertz spectroscopy (TRTS) is a powerful tool for monitoring the injection of an electron into the conduction band of TiO₂.^{14,15} TRTS is an ultrafast, far-infrared technique that is sensitive to the presence of mobile electrons, *i.e.* electrons in the conduction band. By measuring the decrease in the peak amplitude of the THz pulse, the appearance of electrons in the conduction band can be monitored on the fs-ps timescale. Fig. 3 shows the TRTS scans for **Ru1**, **Ru2**, and **Ru3** on TiO₂ in 0.1 M HClO₄. Despite the significant driving force for injection for all three compounds, only **Ru2** and **Ru3** show substantial injection on a one-nanosecond timescale. **Ru1** exhibits less than 20% of the injection amplitude of **Ru3** over the time window permitted by our instrument, despite exhibiting a similar E^{0/}(Ru^{3+/2+*}) potential. A three-exponential function (described in the ESI[†]),

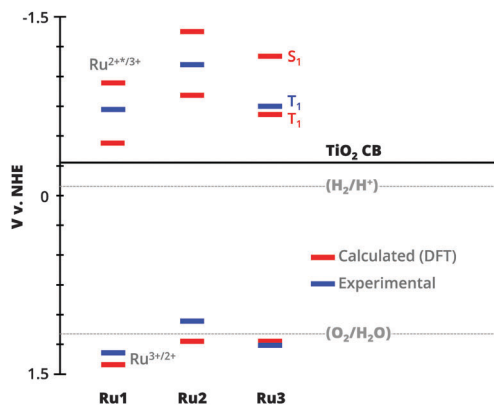


Fig. 1 Experimental and calculated redox potentials for **Ru1**, **Ru2**, and **Ru3** as well as the position of the anatase TiO₂ conduction band and the H₂/H⁺ and O₂/H₂O couples at pH 1.

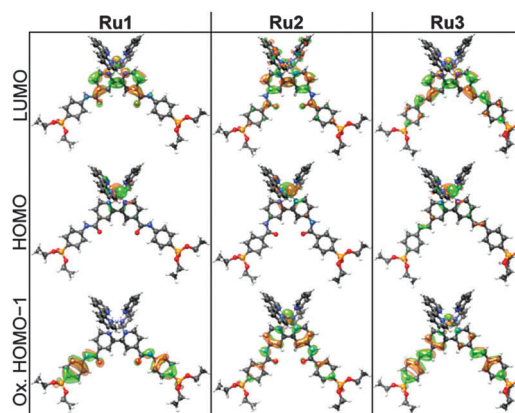


Fig. 2 Ground state HOMO and LUMO of the three esters, along with the HOMO-1 of the structurally relaxed oxidized state. Calculated at the DFT B3LYP/SDD[Ru],6-311+G(d,p)[P,C,N,H,O]/SDD[Ru],6-31G(d)[P,C,N,H,O] level of theory.



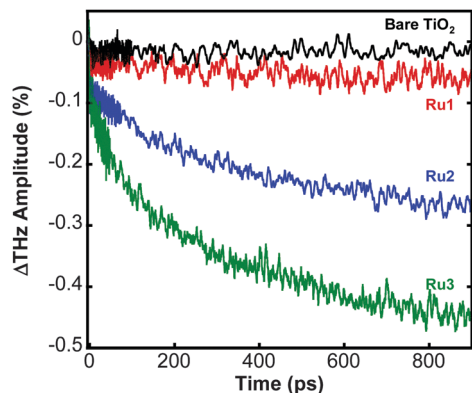


Fig. 3 TRTS scans of **Ru1**, **Ru2**, and **Ru3** on TiO_2 sealed with 0.1 M HClO_4 . Samples were excited with a 100 mW Ti:Sapphire Laser (400 nm, 35 fs, 100 kHz).

convoluted with a Gaussian instrument-response function of 0.5 fs was fitted to the TRTS scans for **Ru2** and **Ru3**. Because of the small injection amplitude of **Ru1**, only a biexponential equation was used for this dye.

All three compounds exhibit a component that is instrument response limited (<0.5 ps). Both **Ru2** and **Ru3** exhibit an intermediate component of 122 ps and 63 ps, respectively, and a slower component of 725 ps and 501 ps, respectively. **Ru1** exhibited only an additional slow component of 520 ps. The relative injection amplitudes for **Ru2** and **Ru3** agree with our previous study of a phosphonated ruthenium tris(bipyridine) on TiO_2 ,¹⁶ with roughly 20% of the injection occurring at less than 0.5 ps and about 50% of the injection occurring at long timescales (Table S2, ESI[†]). We suggest that the fast (<0.5 ps) component likely relates to “hot injection” from the S_1 state, while the long component (>500 ps) corresponds to injection from the vibrationally and structurally relaxed T_1 state. The intermediate component may then account for mixed S_1 and T_1 injection. Based on this picture, the minimal injection from **Ru1** on the 1 ns timescale suggests that intersystem crossing is much faster than injection from the short-lived S_1 state and the slow injection (~ 6 ns) we observe in the transient absorption experiments (see below) is mostly from T_1 .

The much lower injection yield of **Ru1** on a sub-nanosecond timescale is readily rationalized from its LUMO, which is completely localized on the carbonyl and adjacent bpy, far removed from the anchoring phosphonate and thus from the TiO_2 , see Fig. 2. This localization results from the previously mentioned electron-withdrawing effect of the amide carbonyl group, which stabilizes the bpy-LUMO to the point where it remains unmixed with the remainder of the π system. In **Ru2** and **Ru3**, the bpy LUMO is destabilized by the electron-donating amine and vinylene, raising the bpy-LUMO to an energy similar to the remaining part of the conjugated linker, inducing a delocalization towards the anchor. While linker rigidity can inhibit overlap between the chromophore and the anchor group,¹⁷ that is unlikely to play a role in our case as rotation around the amide and ethylene bridges in **Ru1**, **Ru2**, and **Ru3** is permitted.

A quantification of how this MO property affects the injection was obtained from electron dynamics simulations, following a previously reported methodology¹⁸ based on Extended Hückel semi-empirical calculations. The three dyes were anchored to the (101) plane of a 2D-periodic $\text{Ti}_{128}\text{O}_{256}$ slab of anatase *via* a semi-optimized binding geometry obtained from DFT calculations (Fig. S3, ESI[†]). The initial wave packet was created by populating the adsorbate LUMO, the character of which is verified against the DFT-calculated LUMO (Fig. S4, ESI[†]). Propagation was calculated by integrating the time-dependent Schrödinger equation (eqn (S4), ESI[†]) analytically in time steps of 1.0 fs for 1000 fs. Exponential dampening terms were added to the Ti atoms on the edge and bottom of the slab, reducing the wave packet. The population of the wave packet norm on the adsorbate was then monitored and the remaining fraction of the wave packet tracked to give an estimate of the injection time constant τ , see eqn (S5) (ESI[†]) and Fig. 4. The calculated values of τ obtained for the three dyes: 3724 fs, 1234 fs, and 953 fs for **Ru1**, **Ru2**, and **Ru3**, respectively, are in good agreement with the trend from TRTS. Absolute agreement is not expected due to the approximations in the dynamics calculations, which neglect solvent effects and structural dynamics for example.

Transient absorption spectroscopy (TAS), a time-resolved method for investigating fast (ns–ms) electronic processes,^{19–22} allowed us to monitor the recombination of the injected electron back to the oxidized sensitizer on the microsecond time scale (Fig. 5). The samples were excited with a 2 mJ pulse at 532 nm with a beam diameter of 10 mm, and Fig. 5 shows the short (<3 μs) and long (100 μs) single-wavelength traces monitored at 420 nm. At 420 nm, the loss of absorption corresponds to a bleach of the MLCT band following the formation of Ru^{3+} . While the bleach is instantaneous for **Ru2** and **Ru3** on the time scale of the measurement, the bleach grows in on the timescale of several nanoseconds for **Ru1**. A fit of the injection component of the **Ru1** TAS gives an injection lifetime of ~ 6 ns.

A stretched exponential (see ESI[†]) was fit to the data from 100 ns to 100 μs to avoid the contribution from the slow (~ 6 ns) injection observed for **Ru1**. For **Ru1** the value of $\langle \tau \rangle$

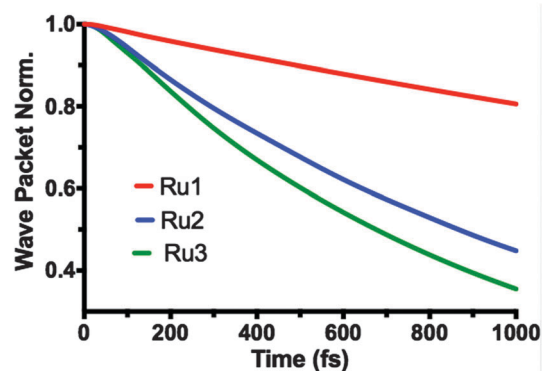


Fig. 4 Extended Hückel dynamics results. The norm of the wave packet plotted in time showing the portion of the original wave packet remaining in the system (*i.e.* that which has not yet been drawn out of the system by the adsorbing boundary conditions).



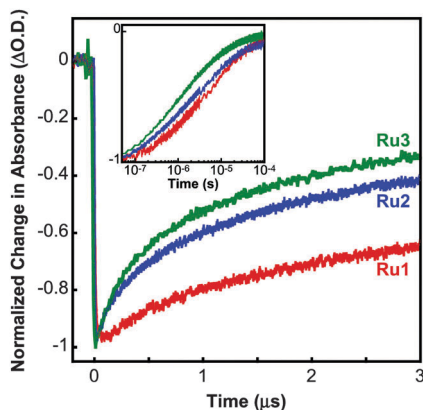


Fig. 5 Transient absorption traces at 420 nm for **Ru1**, **Ru2**, and **Ru3** on TiO_2 in 0.1 M HClO_4 . Samples were excited with a 2 mJ, 532 nm pulse (7 ns, 10 mm, 10 Hz). Inset: absorbance change on a logarithmic time scale that extends to 100 μs .

was $23 \pm 4 \mu\text{s}$, while for **Ru2** and **Ru3** (τ) was $13 \pm 2 \mu\text{s}$ and $7 \pm 2 \mu\text{s}$, respectively. The trend in recombination times from electrons in the TiO_2 to the three oxidized dyes is rationalized from the calculated extents and energies of the HOMO and HOMO–1 of the oxidized dyes. In all dyes, the HOMO is almost exclusively of Ru(4d) character, localized on the ruthenium core. The spatial separation between this orbital and the TiO_2 makes the recombination $\text{TiO}_2 \rightarrow \text{HOMO}_{\text{dye}}$ dominated by Marcus-type hopping due to very weak coupling (eqn (S6), ESI^\dagger), but this type of electron transfer cannot account for the trend in recombination rates between the dyes. While absent in **Ru1**, a more efficient pathway for recombination appears in **Ru2** and **Ru3**, where the HOMO–1 of the oxidized species extends across the entirety of the linkers while also exhibiting significant overlap with the HOMO, see Fig. 2. The hole in the oxidized species can easily access the HOMO–1 in **Ru2** and **Ru3**, where a Boltzmann estimate based on the orbital energies suggests that the population ratio of HOMO–1/HOMO is 0.15%, 1.10%, and 5.73% at 298 K for **Ru1**, **Ru2**, and **Ru3**, respectively. **Ru1** consequently has its recombination quenched for two reasons: the HOMO–1 is too deep to be accessible for the hole on the oxidized dye, and it does not overlap spatially with the HOMO.

In order to gauge the interplay of injection and recombination in these sensitizers, we utilized them as sensitizers in DSSCs (Table S3, ESI^\dagger). Of the three sensitizers, **Ru2** exhibited the highest short-circuit current, open-circuit voltage, and power conversion efficiency. This suggests that the partial conjugation found in **Ru2** provides a better balance of injection and recombination in an actual device than the less conjugated (**Ru1**) or fully conjugated (**Ru3**) sensitizers.

To summarize, we have used advanced time-resolved spectroscopic techniques in conjunction with steady-state and time-dependent quantum chemistry calculations to follow the electronic dynamics of three new light-harvesting sensitizers in which the energy-level landscape is tuned *via* small alterations in the chemical structure of the linkers. The linkers impose notable changes in the rates of injection and recombination when

anchoring the sensitizers to TiO_2 nanoparticles. Dye-sensitized solar cells constructed from these systems show markedly distinct efficiencies. In a broader context, the balance of injection and recombination dynamics being tunable by tailoring the degree of conjugation is likely to be important for many electron-transfer processes beyond dye-sensitized solar cells and water-splitting dye cells.

Acknowledgements

This work was funded by the U.S. Department of Energy Office of Science, Office of Basic Energy Sciences, under award no. DE-FG02-07ER15909 and by a generous donation from the TomKat Charitable Trust. V. S. B. acknowledges support for the computational work from the Argonne-Northwestern Solar Energy Research (ANSER) Center, an Energy Frontier Research Center funded by the U.S. Department of Energy, Office of Science, Office of Basic Energy Sciences (US DOE-OS-BES) under award no. DE-SC0001059 and the Center for High Performance Computing, Shanghai Jiao Tong University.

Notes and references

- 1 J. R. Swierk and T. E. Mallouk, *Chem. Soc. Rev.*, 2013, **42**, 2357–2387.
- 2 K. J. Young, L. A. Martini, R. L. Milot, R. C. Snoberger III, V. S. Batista, C. A. Schmittenmaer, R. H. Crabtree and G. W. Brudvig, *Coord. Chem. Rev.*, 2012, **256**, 2503–2520.
- 3 F. Odobel, L. Le Pleux, Y. Pellegrin and E. Blart, *Acc. Chem. Res.*, 2010, **43**, 1063–1071.
- 4 J. R. Swierk, N. S. McCool and T. E. Mallouk, *J. Phys. Chem. C*, 2015, **119**, 13858–13867.
- 5 Y. Wu and W. Zhu, *Chem. Soc. Rev.*, 2013, **42**, 2039–2058.
- 6 S. Mathew, A. Yella, P. Gao, R. Humphry-Baker, B. F. E. Curchod, N. Ashari-Astani, I. Tavernelli, U. Rothlisberger, M. K. Nazeeruddin and M. Grätzel, *Nat. Chem.*, 2014, **6**, 242–247.
- 7 M. Liang and J. Chen, *Chem. Soc. Rev.*, 2013, **42**, 3453–3488.
- 8 C. Zafer, M. Kus, G. Turkmen, H. Dincalp, S. Demic, B. Kuban, Y. Teoman and S. Icli, *Sol. Energy Mater. Sol. Cells*, 2007, **91**, 427–431.
- 9 W. Ding, C. F. A. Negre, J. L. Palma, A. C. Durrell, L. J. Allen, K. J. Young, R. L. Milot, C. A. Schmittenmaer, G. W. Brudvig, R. H. Crabtree and V. S. Batista, *ChemPhysChem*, 2014, **15**, 1138–1147.
- 10 K. Hanson, M. K. Brennaman, H. Luo, C. R. K. Glasson, J. J. Concepcion, W. Song and T. J. Meyer, *ACS Appl. Mater. Interfaces*, 2012, **4**, 1462–1469.
- 11 K. Hanson, M. K. Brennaman, A. Ito, H. Luo, W. Song, K. A. Parker, R. Ghosh, M. R. Norris, C. R. K. Glasson, J. J. Concepcion, R. Lopez and T. J. Meyer, *J. Phys. Chem. C*, 2012, **116**, 14837–14847.
- 12 H. Park, E. Bae, J.-J. Lee, J. Park and W. Choi, *J. Phys. Chem. B*, 2006, **110**, 8740–8749.
- 13 J. B. Asbury, Y. Q. Wang, E. Hao, H. N. Ghosh and T. Lian, *Res. Chem. Intermed.*, 2001, **27**, 393–406.



- 14 M. C. Beard, G. M. Turner and C. A. Schmuttenmaer, *Phys. Rev. B: Condens. Matter Mater. Phys.*, 2000, **62**, 15764–15777.
- 15 G. M. Turner, M. C. Beard and C. A. Schmuttenmaer, *J. Phys. Chem. B*, 2002, **106**, 11716–11719.
- 16 J. R. Swierk, N. S. McCool, C. T. Nemes, T. E. Mallouk and C. A. Schmuttenmaer, *J. Phys. Chem. C*, 2016, **120**, 5940–5948.
- 17 Z. Yao, L. Ying, C. Yan, M. Zhang, N. Cai, X. Dong and P. Weng, *J. Phys. Chem. C*, 2014, **118**, 2977–2986.
- 18 L. G. C. Rego and V. S. Batista, *J. Am. Chem. Soc.*, 2003, **125**, 7989–7997.
- 19 S. A. Haque, Y. Tachibana, R. L. Willis, J. E. Moser, M. Grätzel, D. R. Klug and J. R. Durrant, *J. Phys. Chem. B*, 2000, **104**, 538–547.
- 20 F. Ma, M. Jarenmark, S. Hedström, P. Persson, E. Nordlander and A. Yartsev, *RSC Adv.*, 2016, **6**, 20507–20515.
- 21 M. K. Brennaman, A. O. T. Patrocinio, W. Song, J. W. Jurss, J. J. Concepcion, P. G. Hoertz, M. C. Traub, N. Y. M. Iha and T. J. Meyer, *ChemSusChem*, 2011, **4**, 216–227.
- 22 P. G. Johansson, Y. Zhang, M. Abrahamsson, G. J. Meyer and E. Galoppini, *Chem. Commun.*, 2011, **47**, 6410–6412.



Molecular Design of Light-Harvesting Photosensitizers: Effect of Varied Linker Conjugation on Interfacial Electron Transfer

Jianbing Jiang[†], John R. Swierk[†], Svante Hedström, Adam J. Matula, Robert H. Crabtree*, Victor S. Batista**,
Charles A. Schmuttenmaer* and Gary W. Brudvig*

Department of Chemistry and Energy Sciences Institute, Yale University, New Haven, Connecticut, 06520,
USA

Table of Contents

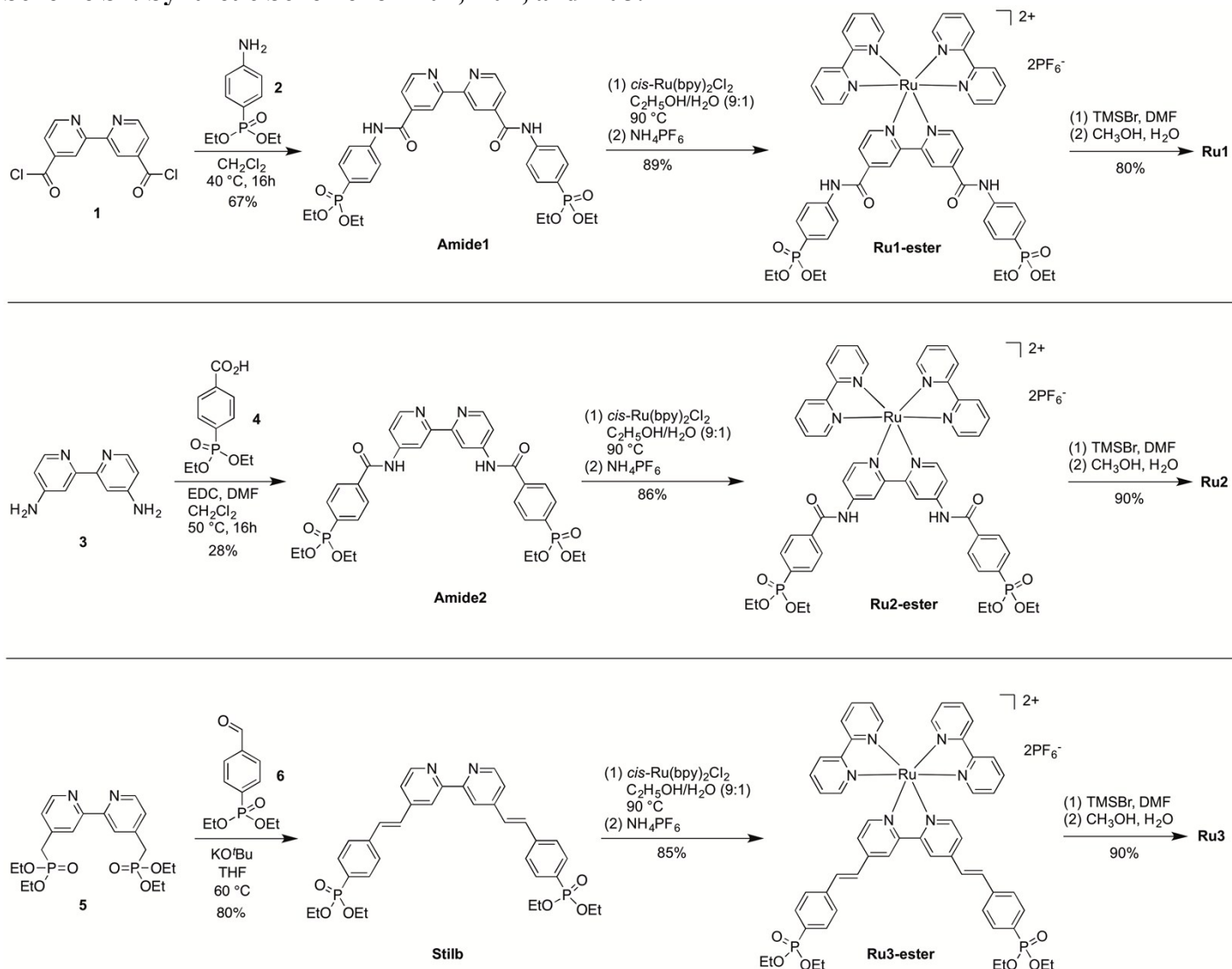
Experimental Details	S2
Scheme S1: Synthetic Scheme for Ru1 , Ru2 , and Ru3	S2
Preparation of Ru1 , Ru2 , and Ru3	S2
Sample Preparation.....	S4
Transient Absorption Measurements.....	S5
Time-Resolved Terahertz (THz) Spectroscopy (TRTS)	S5
Electrochemistry.....	S5
Dye-Sensitized Solar Cells	S6
Figure S1: Steady State Absorption Spectra	S6
Figure S2: CV of Compounds	S6
Table S1: Experimental and Calculated Oxidation and Excited State Reduction Potentials ...	S7
Table S2: Fit Parameters for TRTS Scans.....	S7
Table S3: DSSC Performance Parameters	S7
DFT Calculations.....	S7
Extended Hückel Dynamics Results	S7
Figure S3: Dye–Ti ₁₂₈ O ₂₅₆ systems for the injection dynamics calculations	S8
Figure S4: Extended Hückel LUMOs for Ru , Ru2 , and Ru3	S9
References	S10

Experimental Details

Methods. All chemicals and solvents were commercially available and used as obtained, without further purification. ^1H NMR spectra were recorded at 400 MHz, and ^{13}C NMR spectra were recorded at 100 MHz. Chemical shifts are reported as ppm from the internal reference tetramethylsilane (TMS). High-resolution mass spectrometry (HRMS) was performed on a Q-TOF LC-MS with API by direct injection of a methanolic solution at ~ 0.5 mg/mL concentration. Steady-state absorption spectra were recorded on a Varian Cary 50 Bio UV-visible spectrophotometer. Fluorescence spectra were recorded on a Shimadzu RF-5301pc spectrofluorophotometer. Compounds **1**,¹ **2**,² **3**,³ **4**,⁴ **5**,⁵ and **6**⁶ were prepared according to reported procedures.

Characterization. All compounds were characterized by ^1H NMR and HR-MS. The Ruthenium complexes (esters) were characterized by steady-state absorption and fluorescence spectrometry. ^{13}C NMR spectra were also recorded for compounds **Amide1** and **Stilb**, but not for others due to insufficient solubility.

Scheme S1: Synthetic Scheme for Ru1, Ru2, and Ru3.



Amide1. A solution of **2** (963 mg, 4.20 mmol) in CH₂Cl₂ (5.0 mL) was added to a solution of 4,4'-di(chlorocarbonyl)-2,2'-bipyridine **1** (556 mg, 2.0 mmol) in CH₂Cl₂ (5.0 mL). A pink precipitate formed immediately after addition. The mixture was heated to 40 °C and stirred under nitrogen for 16 h. The suspension was centrifuged, and the supernatant was discarded. The crude residue was washed successively with 1 N HCl, water and CH₂Cl₂. The product was dried to afford the title compound as a pink solid. (892 mg, 67%). ¹H NMR (CDCl₃), 1.23 (t, *J* = 7.0 Hz, 12H), 3.93–4.07 (m, 8H), 7.72 (d, *J* = 12 Hz, 2H), 7.74 (d, *J* = 12 Hz, 2H), 7.99 (m, 6H), 8.91 (s, 2H), 8.96 (d, *J* = 4.0 Hz, 2H), 10.97 (s, 2H); ¹³C NMR (CD₃OD + CDCl₃), 19.8, 66.4, 123.2, 124.2, 126.1, 136.5, 146.4, 147.5, 154.0, 160.1, 169.2; ESI-MS obsd 667.1946, calcd 667.2081 [(M + H)⁺, M = C₃₂H₃₆N₄O₈P₂].

Ru1-ester. A solution of **Amide1** (333 mg, 0.5 mmol) and *cis*-[Ru(bpy)₂Cl₂] (260 mg, 0.5 mmol) in a solvent mixture of C₂H₅OH and H₂O (30 mL, 9:1, v/v) was stirred at 90 °C under nitrogen for 20 h. The solvents were removed by rotary evaporation. The dark residue was dissolved in a minimum amount of water and CH₃CN (~2.0 mL, 1:1, v/v) and loaded to a LH20 column. Pure CH₃CN was first used to remove the unreacted *cis*-[Ru(bpy)₂Cl₂], and then changed to 7% of CH₃OH in CH₃CN. The dark orange band was collected. The solvents were removed by rotary evaporation. The residue was dissolved in a minimum amount of water (~2.0 mL), and then a saturated solution of NH₄PF₆ (~20 mL) was added. The suspension was centrifuged, and the supernatant was discarded to afford a dark orange solid, which was washed twice with water. The solid was dried under high vacuum to afford a dark orange powder. (610 mg, 89%). ¹H NMR (DMSO-*d*₆), 1.23 (t, *J* = 8.0 Hz, 12H), 3.93–4.07 (m, 8H), 7.55 (m, 4H), 7.72–7.80 (m, 8H), 7.91–7.99 (m, 8H), 8.17–8.23 (m, 4H), 8.87 (d, *J* = 8.0 Hz, 4H), 9.39 (s, 2H); ESI-MS obsd 540.1193, calcd 540.1208 (M²⁺, M = C₅₂H₅₂N₈O₈P₂Ru).

Ru1. To a solution of **Ru1-ester** (63 mg, 0.051 mmol) in DMF (2.57 mL) was added TMSBr (81.4 μL, 0.617 mmol, 12 eq) under nitrogen. The solution was stirred under nitrogen at 60 °C in the dark for 18 h. DMF and excess TMSBr were removed under high vacuum at °C. To the orange residue was added a mixture of solvents (8.0 mL CH₃OH + 0.5 mL H₂O) and the mixture was stirred at room temperature for 3 h. Diethyl ether was added to the reaction mixture, the suspension was centrifuged, and the supernatant was discarded to afford an orange solid. The solid was dried under high vacuum to afford a dark orange powder (46.4 mg, 80%). ¹H NMR (DMSO-*d*₆), 7.55 (q, *J* = 8.0 Hz, 4H), 7.66–7.86 (m, 12H), 7.55–7.59 (m, 4H), 8.88 (d, *J* = 8.0 Hz, 4H), 9.43 (s, 2H), 10.93 (s, 4H); ESI-MS obsd 484.0622, calcd 484.0582 (M²⁺, M = C₄₄H₃₆N₈O₈P₂Ru).

Amide2. A sample of phosphanobenzoic acid **4** (1.032 g, 4.0 mmol) and EDC (1.15 g, 6.0 mmol) in CH₂Cl₂ (4.0 mL) was stirred at room temperature under nitrogen for 40 min (Solution A). In a separate vial, diaminodipyridine **3** (372 mg, 2.0 mmol) was dissolved in DMF (3 mL) and stirred for 3 min (Solution B). Solution B was then transferred via pipette to solution A. The resulting mixture was stirred under nitrogen at 50 °C for 16 h. To the crude mixture was added water, and the precipitate was isolated and washed successively with 1 N HCl, saturated NaHCO₃ and hexanes. The grey solid was dried to afford the title compound (747 mg, 28%). ¹H NMR (CDCl₃), 1.24 (t, *J* = 7.0 Hz, 12H), 4.00–4.12 (m, 8H), 7.88 (d, *J* = 12.0 Hz, 2H), 7.90 (d, *J* = 12.0 Hz, 2H), 7.94 (dd, *J*₁ = 8.0 Hz, *J*₂ = 3.0 Hz, 2H), 8.62 (d, *J* = 8.0 Hz, 2H), 8.85 (d, *J* = 4.0 Hz, 2H), 10.90 (s, 2H); ESI-MS obsd 667.2052, calcd 667.2081 [(M + H)⁺, M = C₃₂H₃₇N₄O₈P₂].

Ru2-ester. A solution of **Amide2** (11.1 mg, 0.017 mmol) and *cis*-[Ru(bpy)₂Cl₂] (8.7 mg, 0.017 mmol) in a solvent mixture of ethanol and water (1.0 mL, 9:1, v/v) was stirred at 90 °C under nitrogen for 12 h. The solvents were removed by rotary evaporation. The crude dark residue was dissolved in a minimum amount of water and CH₃CN (~1.0 mL, 1:1, v/v) and loaded to a LH20 column. Pure CH₃CN was first used to remove the reacted *cis*-[Ru(bpy)₂Cl₂], and then changed to 7% of methanol in CH₃CN. The dark orange band was collected. The solvents were removed by rotary evaporation. The residue was dissolved in a minimum amount of water (~1.0 mL), and then a saturated solution of NH₄PF₆ (~10 mL) was added. The precipitate was centrifuged, and the supernatant was discarded to afford a dark orange solid, which was washed twice with water. The solid was dried under high vacuum to afford a dark orange powder (20 mg, 86%). ¹H NMR (DMSO-*d*₆), 1.24 (t, *J* =

8.0 Hz, 12H), 4.00–4.10 (m, 8H), 7.48–7.56 (m, 4H), 7.65 (d, $J = 8.0$ Hz, 2H), 7.71 (d, $J = 8.0$ Hz, 2H), 7.82–7.95 (m, 8H), 8.08–8.18 (m, 8H), 8.83 (d, $J = 8.0$ Hz, 2H), 9.13 (s, 2H); ESI-MS obsd 540.1217, calcd 540.1208 (M^{2+} , $M = C_{52}H_{52}N_8O_8P_2Ru$).

Ru2. To a solution of **Ru2-ester** (25 mg, 0.018 mmol) in DMF (0.91 mL) was added TMSBr (28.9 μ L, 0.219 mmol, 12 eq) under nitrogen. The solution was stirred under nitrogen at 60 °C in the dark for 18 h. DMF and excess TMSBr were removed under high vacuum at 60 °C. To the orange residue was added a mixture of solvents (4.0 mL $CH_3OH + 0.5$ mL H_2O), and the mixture was stirred at room temperature for 6 h. Diethyl ether was added to the reaction mixture, the suspension was centrifuged, and the supernatant was discarded to afford an orange solid. The solid was dried under high vacuum to afford a dark orange powder (46.4 mg, 80%). 1H NMR ($DMSO-d_6$), 7.49–7.56 (m, 4H), 7.65 (d, $J = 8.0$ Hz, 2H), 7.72 (d, $J = 4.0$ Hz, 2H), 7.83–7.89 (m, 8H), 8.03–8.05 (m, 4H), 8.12–8.18 (m, 4H), 8.83 (d, $J = 8.0$ Hz, 2H), 9.14 (s, 2H), 11.31 (s, 4H); ESI-MS obsd 484.0602, calcd 484.0582 (M^{2+} , $M = C_{44}H_{36}N_8O_8P_2Ru$).

Stilb. To a solution of phosphanomethyldipyridine **5** (182 mg, 0.4 mmol) in THF (2 mL) was added KO^tBu (180 mg, 1.6 mmol), and the resulting suspension was stirred under nitrogen for 10 min. Another solution of phosphanobenzaldehyde **4** (290 mg, 1.2 mmol) in THF (2 mL) was transferred to the former solution, and the resulting mixture was stirred under nitrogen for 16 h. Hexanes were added to the reaction mixture, and the precipitate was isolated and washed with water. The solid was dried to afford the title compound as a grey powder (202 mg, 80%). 1H NMR (CD_3OD), 1.34 (t, $J = 8.0$ Hz, 12H), 4.07–4.20 (m, 8H), 7.46 (d, $J = 16.0$ Hz, 2H), 7.65 (d, $J = 16.0$ Hz, 2H), 7.66 (dd, $J_1 = 6.0$ Hz, $J_2 = 2.0$ Hz, 2H), 7.79–7.85 (m, 8H), 8.53 (s, 2H), 8.67 (d, $J = 8.0$ Hz, 2H); ^{13}C NMR ($CD_3OD + CDCl_3$), 16.3, 62.6, 118.8, 121.6, 127.1, 128.8, 132.4, 145.6, 149.7, 156.5; ESI-MS obsd 633.2295, calcd 633.2278 [($M + H$)⁺, $M = C_{34}H_{38}N_2O_6P_2$].

Ru3-ester. A solution of **Stilb** (78.1 mg, 0.123 mmol) and *cis*-[Ru(bpy)₂Cl₂] (64.2 mg, 0.123 mmol) in a solvent mixture of C_2H_5OH and H_2O (7.4 mL, 9:1, v/v) was stirred at 95 °C under nitrogen for 20 h. The solvents were removed by rotary evaporation. The crude dark residue was dissolved in a minimum amount of water and CH_3CN (~2.0 mL, 1:1, v/v) and loaded to a LH20 column. Pure CH_3CN was first used to remove the reacted *cis*-[Ru(bpy)₂Cl₂], then changed to 7% of methanol in CH_3CN . The dark orange band was collected. The solvents were removed by rotary evaporation. The residue was dissolved in a minimum amount of water (~2.0 mL), and then a saturated solution of NH_4PF_6 (~15 mL) was added. The precipitate was centrifuged, and the supernatant was discarded to afford a dark orange solid, which was washed twice with water. The solid was dried under high vacuum to afford a dark orange powder (141 mg, 85%). 1H NMR (CD_3OD), 1.33 (t, $J = 8.0$ Hz, 12H), 4.08–4.17 (m, 8H), 7.46–7.53 (m, 8H), 7.60 (d, $J = 8.0$ Hz, 4H), 7.71–7.83 (m, 16H), 7.93 (d, $J = 8.0$ Hz, 2H), 8.09–8.14 (m, 4H), 8.69 (d, $J = 8.0$ Hz, 4H), 8.96 (s, 2H); ESI-MS obsd 523.1368, calcd 523.1306 (M^{2+} , $M = C_{54}H_{54}N_6O_6P_2Ru$).

Ru3. To a solution of **Ru3-ester** (75 mg, 0.055 mmol) in DMF (2.76 mL) was added TMSBr (87.5 μ L, 0.663 mmol, 12 eq) under nitrogen. The solution was stirred under nitrogen at 60 °C in the dark for 12 h. DMF and excess TMSBr were removed under high vacuum at 60 °C. To the orange residue was added a mixture of solvents (4.0 mL $CH_3OH + 0.5$ mL H_2O), and the mixture was stirred at room temperature for 5 h. Diethyl ether was added to the reaction mixture, the suspension was centrifuged, and the supernatant was discarded to afford an orange solid. The solid was dried under high vacuum to afford a dark orange powder (50.3 mg, 82%). 1H NMR ($DMSO-d_6$), 7.44–7.90 (m, 22H), 8.14 (t, $J = 8.0$ Hz, 4H), 8.79 (d, $J = 8.0$ Hz, 4H); ESI-MS obsd 467.0668, calcd 467.0680 (M^{2+} , $M = C_{46}H_{38}N_6O_6P_2Ru$).

Sample Preparation. TiO_2 films for transient absorption measurements were prepared on TEC15 fluorine-doped tin oxide (FTO) glass (Hartford Glass Co.). An organic TiO_2 paste (Solaronix Ti-Nanoxide T/SP) was doctor-bladed onto the FTO glass using a single layer of Scotch tape as a spacer layer to give a nominal thickness of 1.2 μ m and then then dried at 80 °C for 10 min. After drying, the films were then sintered

in a box furnace at 470 °C for 30 min. The films were sensitized for 16 h in a 0.1 mM solution of dye dissolved in 5:3 0.1M HClO₄:DMSO. Transient absorption measurements were made in 0.1 M HClO₄.

Samples for THz measurements were prepared on fused quartz substrates as described in detail elsewhere.⁷ Briefly, TiO₂ particles were ground with acetic acid, water, and ethanol to form a paste and then ultrasonicated. α -Terpineol and ethyl cellulose were added as binders and the excess ethanol stripped to give a paste. The paste was doctor-bladed onto fused quartz substrates (GM associates) using Scotch tape as a spacer. Each layer was dried at 80 °C before the next layer was added. A total of five layers of TiO₂ were deposited to give a nominal film thickness of 6 μ m. The films were sensitized as above and afterwards sealed using a second piece of quartz separated by a 60 μ m Surlyn spacer (Solaronix). 0.1 M HClO₄ was introduced into the gap between the pieces of quartz via vacuum backfilling.

Transient Absorption Measurements. Nanosecond transient absorption measurements were made using an Edinburgh Instruments LP920 Transient Absorbance Spectrometer. The sample was pumped at 530 nm (2 mJ/pulse) by a Nd:YAG laser (Spectra-Physics INDI-10) passed through an OPO (Spectra-Physics basiScan M). A pulsed 450 W Xe arc lamp was utilized as the probe source. Prior to the sample, the probe was filtered through a 450 nm short pass filter. After the sample, the probe light was passed through a monochromator and into a photomultiplier tube. Changes in absorbance were monitored at 420 nm. Typically 64 shots were averaged and the data were fit to a stretched exponential equation of the form:

$$\Delta A = \Delta A_0 \exp \left[- \left(\frac{t}{\tau} \right)^\beta \right] + c \quad (\text{S1})$$

where ΔA_0 is the change in absorbance at $t = 0$, τ is the lifetime, β is a stretching parameter ($0 < \beta \leq 1$), and c is an offset at long times. When $\beta = 1$, the equation becomes a single exponential with an offset. The lifetime τ can be used to calculate a rate constant for recombination (k_{obs}) and a weighted lifetime for recombination ($\langle \tau \rangle$) can be calculated from:

$$\langle \tau \rangle = \frac{1}{k_{obs} \beta} \Gamma \left(\frac{1}{\beta} \right) \quad (\text{S2})$$

Time-Resolved Terahertz (THz) Spectroscopy (TRTS). The THz spectrometer and technique is described in detail elsewhere.⁸⁻⁹ Briefly, the 35 fs, 800 nm output of an amplified Ti:sapphire laser (Spectra-Physics) operating a repetition rate of 1 kHz is split into a THz generation beam, a detection beam, and a pump beam. The generation beam is frequency doubled and along with the fundamental harmonic focused in air to generate a plasma.^{10,11} The pump beam is likewise frequency doubled to 400 nm and adjusted using a variable neutral density filter to obtain a power of 100 mW (100 μ J/pulse) at a spot size of 10 mm. Before the sample, the laser is passed through a 5 mm diameter aperture. The forward propagating THz pulse generated by the plasma is collected and focused using a series of off-axis paraboloidal mirrors. THz radiation is detected with a ZnTe(110) crystal using free-space electro-optic sampling.¹² The instrument response function was given by a Gaussian function with a full-width at half-maximum of 500 fs and the TRTS scans fit with the following function:

$$\Delta THz = \left\{ \Delta THz_0 + \sum_{i=1}^n A_i \left[\exp \left(- \frac{t-t_0}{\tau_i} \right) - 1 \right] \right\} \otimes G(FWHM) \quad (\text{S3})$$

where THz_0 is a baseline offset, n is the number of exponential terms used in the fit, A_i is the injection amplitude of a given component, t_0 is the arrival time of the pump pulse, $G(FWHM)$ represents a normalized Gaussian instrument response function, and \otimes is a convolution.

Electrochemistry. The ester versions of Ru1, Ru2, and Ru3 were dissolved in acetonitrile to give a 10 mM solution. Tetrabutylammonium perchlorate was used as a supporting electrolyte (0.1 M). A platinum disk electrode was used as the working electrode and a piece of platinum mesh was used as the counter electrode. A silver wire was utilized as a quasi-reference and the potentials measured relative to ferrocene (0.64 V vs. NHE). The potential was swept at a rate of 10 mV/s.

Dye-Sensitized Solar Cells. DSSCs were fabricated as previously reported.¹³ Briefly, a TiO_2 blocking layer was applied to a piece of TEC7 FTO glass (Hartford Glass co.) by immersion in a 40 mM aqueous solution of $TiCl_4 \cdot THF$ for 30 min at 80 °C before being crystallized at 570 °C for 10 min. An organic TiO_2 paste (Solaronix Ti-Nanoxide T/SP) was doctor-bladed on the substrates using Scotch tape as a spacer layer and cured at 80 °C for 10 min to give a nominal layer thickness of 4 μm . A total of 3 layers were applied to give a TiO_2 thickness of approximately 12 μm . The films were sintered at 470 °C for 30 min and treated again with $TiCl_4 \cdot THF$ as before being immersed in a 0.1 mM dye solution in 5:3 0.1M $HClO_4$:DMSO for 16 h. Platinum cathodes were prepared by doctor blading an 8 wt% solution of H_2PtCl_6 in ethanol on TEC15 FTO glass and then annealed at 450 °C for 30 min. The anode and cathode were hot-pressed together using a 60 μm Surlyn spacer (Solaronix) and vacuumed backfilled with electrolyte (Iodolyte HI-30).

The photovoltaic characteristics of the solar cells were tested using a solar simulator fitted with an AM-1.5 filter and calibrated using a Si reference diode.

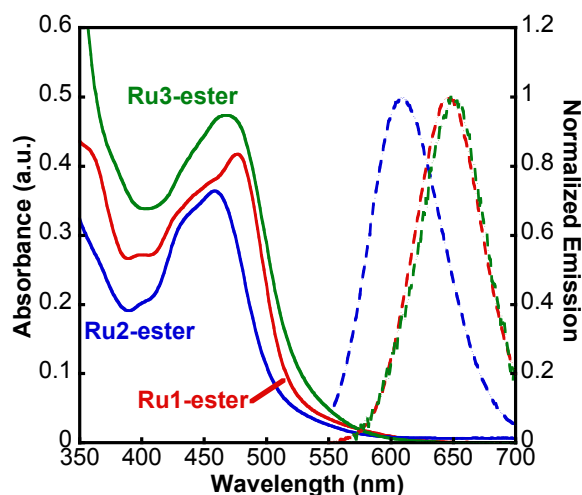


Figure S1: Steady-state absorption spectra (solid line) and emission spectra (dashed lines) of 25 μM **Ru1-ester**, **Ru2-ester**, and **Ru3-ester** in acetonitrile.

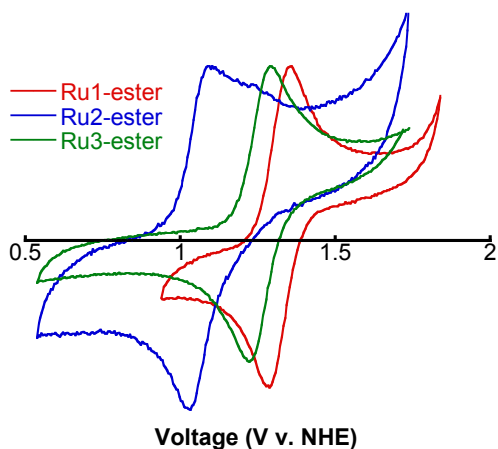


Figure S2: Cyclic voltammograms of **Ru1-ester**, **Ru2-ester**, and **Ru3-ester** (10 mM) in acetonitrile (0.1 M tetrabutylammonium perchlorate). Pt disk working electrode, Pt mesh counter electrode, Ag wire quasi-referenced to ferrocene (0.64 V vs. NHE).

Table S1: Experimental and Calculated Ground State Potentials for Oxidation vs. NHE and Excited State Potentials

	Experimental			Calculated				
	Ru ^{2+/3+}	E ₀₋₀	Ru ^{3+/2+*}	Ru ^{2+/3+}	E _{vert} (S ₁)	Ru ^{3+/2+*} (S ₁)	E _{opt} (T ₁)	Ru ^{3+/2+*} (T ₁)
Ru1	1.32	1.95	-0.63	1.39	2.31	-0.92	1.82	-0.43
Ru2	1.06	2.08	-1.02	1.19	2.55	-1.36	2.05	-0.86
Ru3	1.21	1.93	-0.72	1.20	2.33	-1.13	1.84	-0.64

Electrochemical potentials vs. NHE, E₀₋₀ values are reported in eV

Table S2: Fit parameters for TRTS scans

	A ₁	τ ₁ (ps)	A ₂	τ ₂ (ps)	A ₃	τ ₃ (ps)	THz ₀	t ₀ (ps)	Scaling Factor
Ru1	0.51	<0.5	0.49	520			0.00	-0.20	0.07
Ru2	0.22	< 0.5	0.23	122	0.55	725	0.00	-0.31	0.32
Ru3	0.18	< 0.5	0.27	63	0.55	501	0.00	-0.23	0.50

Table S3: Operating parameters for DSSCs

	J _{sc} (mA cm ⁻²)	V _{oc} (mV)	FF	η (%)
Ru1	0.61 ± 0.02	500 ± 25	0.52 ± 0.07	0.16 ± 0.03
Ru2	0.91 ± 0.03	506 ± 49	0.55 ± 0.11	0.26 ± 0.07
Ru3	0.79 ± 0.12	486 ± 18	0.43 ± 0.03	0.17 ± 0.04
N719	13.85 ± 0.59	637 ± 0	0.52 ± 0.07	5.23 ± 0.10

DFT calculations. All DFT calculations were performed with the Gaussian09 software¹⁴ and the B3LYP exchange–correlation density functional.¹⁵ Optimizations of the S_0 ground state, the T_1 state, and the oxidized state were performed with the SDD basis set and effective core potential on ruthenium and the 6-31G(d) basis set¹⁶ on the remaining atom types. The solvent was represented by a polarizable continuum model of DMSO, using the default settings in Gaussian09. All optimizations were followed by single point calculations with the SDD[Ru]/6-311+G(d,p)[C,H,N,O,P] triple zeta basis set to obtain the state potentials as well as the distributions and energies of the molecular orbitals. Linear-response time-dependent DFT calculations using SDD[Ru]/6-31G(d)[C,H,N,O,P] were used to calculate the $S_0 \rightarrow S_1$ vertical excitation.

Electron injection dynamics. The electron injection from dye to TiO_2 was modeled computationally with a quantum dynamics simulation based on an extended Hückel methodology as previously reported.¹⁷ The binding geometry was first obtained from a system with a $\text{CH}_3\text{-PO}_3^{2-}$ anchor group chemisorbed in a bidentate fashion to the (101) surface of a $\text{Ti}_7\text{O}_{27}\text{H}_{28}^{2+}$ cluster. This was subjected to a structural optimization using the PBE functional¹⁸ and the Def2SV(P) basis set and density fitting basis set,¹⁹ with all Ti and O atoms frozen in the anatase crystal structure, except the 6 atoms closest to the adsorbate which were allowed to structurally relax together with the methylphosphonate. Using the resulting semi-optimized binding geometry, the 3 dyes in their S_0 geometry were attached to the (101) surface of a $\text{Ti}_{128}\text{O}_{256}$ slab of anatase in its crystal geometry.

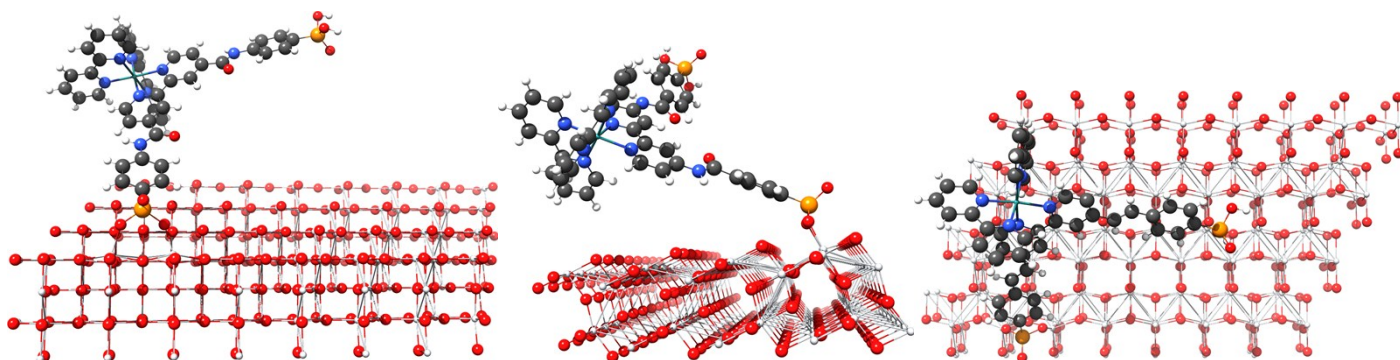


Figure S3. Dye– $\text{Ti}_{128}\text{O}_{256}$ systems for the injection dynamics calculations. **Ru1** front view, **Ru2** side view, **Ru3** top-view.

The propagation of the wave function of an electron starting in the adsorbate LUMO was then calculated by solving the time-dependent Schrödinger Equation:

$$|\Psi(t)\rangle = |\Psi(t)\rangle = \sum_k \left\langle \phi_k \left| \Psi(0) e^{-\frac{iE_k t}{\hbar}} \right| \phi_k \right\rangle$$

$$|\Psi(t)\rangle = \sum_k \left\langle \phi_k \left| \Psi(0) e^{-\frac{iE_k t}{\hbar}} \right| \phi_k \right\rangle \quad (\text{S4})$$

Here $|\Psi(0)\rangle$ is the initial wave function with the wave packet in the adsorbate LUMO, the ϕ_k are the molecular orbitals with associated eigenvalues E_k that make up the total wave function, obtained from extended Hückel calculations using the YaEHMOP software.²⁰ The wave function at time t , $|\Psi(t)\rangle$, was calculated in time steps of 1.0 fs for a total of 1000 fs while monitoring the projection of this wave packet on the TiO_2 basis functions. Exponential dampening absorbing boundary potentials were placed on the sides and bottom of the TiO_2 slab to prevent artificial electron back-transfer events from occurring. These events are known to occur when using PBCs to calculate the energy levels of the TiO_2 , and by removing the wave packet from the system when they reach the orbitals of the marked Ti atoms we can prevent them while measuring the overall injection. The norm

of the wave packet decreases when the wave packet density reaches an orbital to which the adsorbing potentials have been applied. To determine the time constant from the dynamics calculations, we fitted an exponential function of time to the decaying wave packet norm:

$$Norm_{WavePacket}(t) = e^{-\frac{t}{\tau}} \quad (S5)$$

Extended Hückel calculations tend to describe the electronic structure within a single material well but, because the semiempirical energy parameters used in the method are referenced to different vacuum states, when combining two or more types of materials it is important to realign the relevant energy levels. Here, we shifted the adsorbate molecular orbitals towards higher energies as necessary to confer an injection driving force of the same magnitude as observed experimentally.

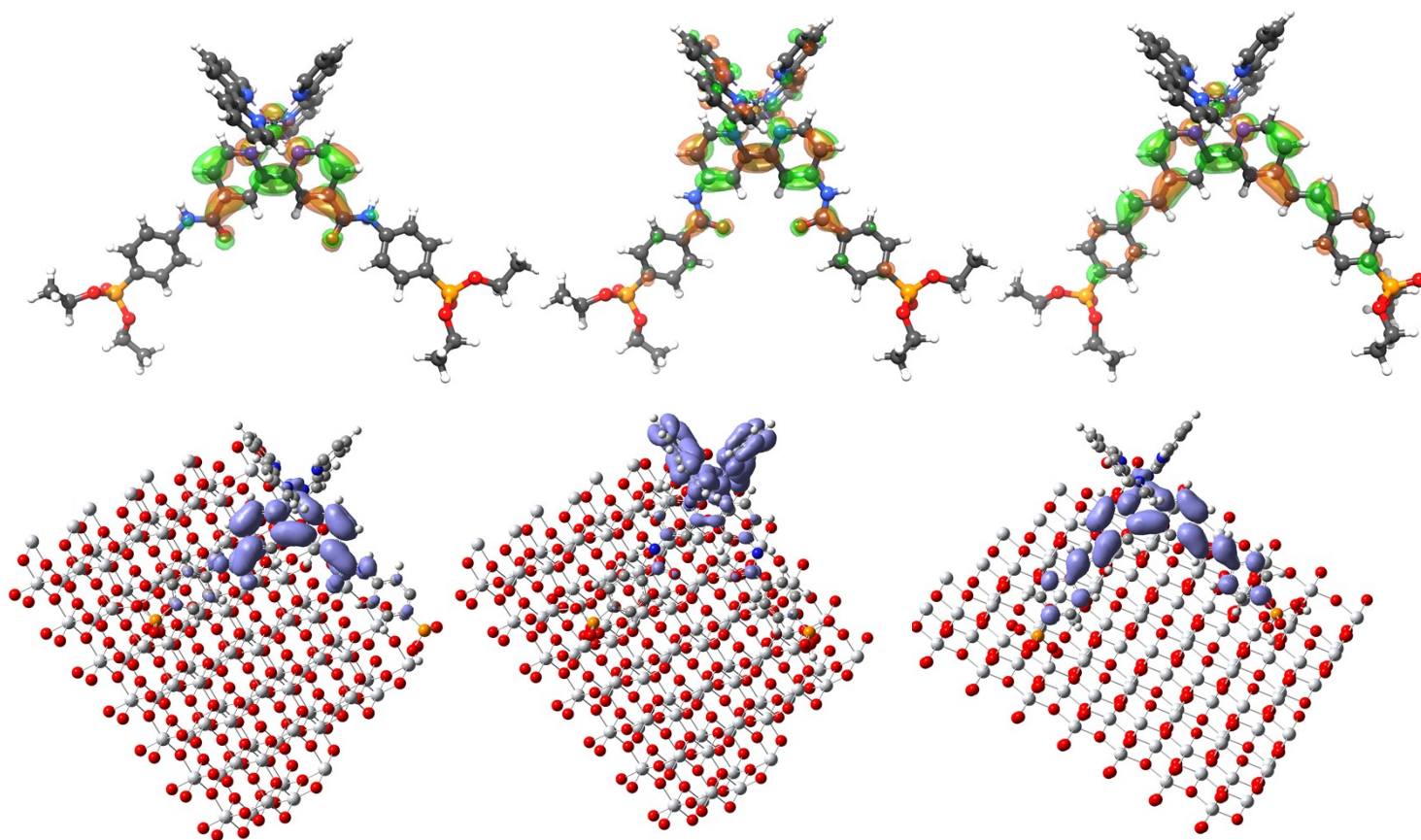


Figure S4. (Top) DFT LUMOs for the ester versions of the dyes. Very good agreement is obtained between the two methods. (Bottom) Extended Hückel LUMOs for **Ru**, **Ru2**, and **Ru3** on the $Ti_{128}O_{256}$ slab.

Marcus-type recombination. An attempt was made at estimating the relative recombination rates with a Marcus-type hopping equation, assuming a constant donor state potential, E_{D,TiO_2} , and a constant coupling, H_{AD} , between the TiO_2 donor state and the dye HOMO acceptor state. This reduces the Marcus prefactor, and yields the following equation for relative rates:

$$\frac{k_1}{k_2} = \sqrt{\frac{\lambda_1}{\lambda_2}} \exp\left(-\frac{(\Delta G_1 + \lambda_1)}{4\lambda_1 k_B T} + \frac{(\Delta G_2 + \lambda_2)}{4\lambda_2 k_B T}\right), \quad \Delta G = E_{HOMO} - E_{D, TiO_2} \quad (S6)$$

The acceptor HOMO potentials, E_{HOMO} , were obtained from the DFT calculations on the isolated ester versions of the neutral dyes, while the outer-sphere reorganization energies, λ , were obtained by considering the potentials of four states: 1) the fully optimized oxidized dye, 2) the fully optimized neutral dye, 3) the oxidized dye at the geometry and non-equilibrium PCM solvent shell of the neutral dye, and 4) the neutral dye at the geometry and non-equilibrium PCM solvent shell of the oxidized dye. This results in values of λ of 0.633, 0.626, and 0.610 eV for **Ru1**, **Ru2**, and **Ru3**, respectively. However, the correct recombination rate trend between the three dyes is only observed for $E_{D, TiO_2} \approx -5.5$ eV vs. vacuum, deeper than physically sensible. It is, therefore, concluded that the recombination occurs not only via direct hopping from TiO_2 to the oxidized dye HOMO, but also through some other mechanism.

References

1. Khatua, S. and Schmittel, M, *Org. Lett.* 2013, **15**, 4422–4425.
2. Nemeth, G, *J. Med. Chem.*, 2014, **57**, 3939–3965.
3. Adams, C. J., Bowen, L. E., Humphrey, M. G., Morrall, J. P. L., Samoc, M. and Yellowlees, L. J., *Dalton Trans.*, 2004, 4130–4138.
4. Beletskaya, I. P., Kabachnik, M. M. and Solntseva, M. D., *Russ. J. Org. Chem.*, 1999, **35**, 71–73.
5. I. Gillaizeau-Gauthier, F. Odobel, M. Alebbi, R. Argazzi, E. Costa, C. A. Bignozzi, P. Qu and G. J. Meyer, *Inorg. Chem.*, 2001, **40**, 6073–6079.
6. Hau, S. K., Cheng, Y.–J., Yip, H.–L., Zhang, Y., Ma, H. Jen, A. K.–Y., *ACS Appl. Mater. Inter.*, 2010, **2**, 1892–1902.
7. J. R. Swierk, N. S. McCool, C. T. Nemes, T. E. Mallouk and C. A. Schmuttenmaer, *J. Phys. Chem. C*, 2016, acs.jpcc.6b00749.
8. M. C. Beard, G. M. Turner and C. A. Schmuttenmaer, *Phys. Rev. B*, 2000, **62**, 15764–15777.
9. C. T. Nemes, C. Koenigsmann and C. A. Schmuttenmaer, *J. Phys. Chem. Lett.*, 2015, **6**, 3257–3262.
10. D. J. Cook and R. M. Hochstrasser, *Opt. Lett.*, 2000, **25**, 1210–1212.
11. T. Bartel, P. Gaal, K. Reimann, M. Woerner and T. Elsaesser, *Opt. Lett.*, 2005, **30**, 2805–2807.
12. Q. Wu and X. C. Zhang, *Appl. Phys. Lett.*, 1995, **67**, 3523–3525.
13. C. Koenigsmann, T. S. Ripolles, B. J. Brennan, C. F. A. Negre, M. Koepf, A. C. Durrell, R. L. Milot, J. A. Torre, R. H. Crabtree, V. S. Batista, G. W. Brudvig, J. Bisquert and C. A. Schmuttenmaer, *Phys Chem Chem Phys*, 2014, **16**, 16629–16641.
14. Gaussian 09, Revision D.01, Frisch, M. J.; Trucks, G. W.; Schlegel, H. B.; Scuseria, G. E.; Robb, M. A.; Cheeseman, J. R.; Scalmani, G.; Barone, V.; Mennucci, B.; Petersson, G. A.; Nakatsuji, H.; Caricato, M.; Li, X.; Hratchian, H. P.; Izmaylov, A. F.; Bloino, J.; Zheng, G.; Sonnenberg, J. L.; Hada, M.; Ehara, M.; Toyota, K.; Fukuda, R.; Hasegawa, J.; Ishida, M.; Nakajima, T.; Honda, Y.; Kitao, O.; Nakai, H.; Vreven, T.; Montgomery, J. A., Jr.; Peralta, J. E.; Ogliaro, F.; Bearpark, M.; Heyd, J. J.; Brothers, E.; Kudin, K. N.; Staroverov, V. N.; Kobayashi, R.; Normand, J.; Raghavachari, K.; Rendell, A.; Burant, J. C.; Iyengar, S. S.; Tomasi, J.; Cossi, M.; Rega, N.; Millam, J. M.; Klene, M.; Knox, J. E.; Cross, J. B.; Bakken, V.; Adamo, C.; Jaramillo, J.; Gomperts, R.; Stratmann, R. E.; Yazyev, O.; Austin, A. J.; Cammi, R.; Pomelli, C.; Ochterski, J. W.; Martin, R. L.; Morokuma, K.; Zakrzewski, V. G.; Voth, G. A.; Salvador, P.; Dannenberg, J. J.; Dapprich, S.; Daniels, A. D.; Farkas, Ö.; Foresman, J. B.; Ortiz, J. V.; Cioslowski, J.; Fox, D. J. Gaussian, Inc., Wallingford CT, 2009.
15. Becke, A.D., *J. Chem. Phys.*, 1993, **98**, 5648-5652.
16. Ditchfield, R. H. W. J., W. J. Hehre, and John A. Pople, *J. Chem Phys.*, 1971, **54**, 724-728.
17. L. G. C. Rego and V. S. Batista, *J. Am. Chem. Soc.*, 2003, **125**, 7989–7997.
18. Perdew, J. P., Burke, K., Ernzerhof, M., *Phys. Rev. Lett.*, 1996, **77**, 3865.
19. Weigend, F., Ahlrichs, R., *Phys. Chem. Chem. Phys.*, 2005, **7**, 3297-3305.
20. G.A.Landrum and W.V.Glassey, **bind** 3.0. in YAeHMOP, overlap.chem.cornell.edu:8080/yaehmop.html